Modified denatured lysozyme effectively solubilizes fullerene c60 nanoparticles in water

IOP Publishing Nanotechnology
Nanotechnology **28** (2017) 335601 (14pp) https://doi.org/10.1088/1361-6528/aa744e

Modified denatured lysozyme effectively solubilizes fullerene c60 nanoparticles in water

Marialuisa Siepi[1], Jane Politi[2], Principia Dardano[2], Angela Amoresano[3], Luca De Stefano[2], Daria Maria Monti[3] and Eugenio Notomista[1]

[1] Department of Biology University of Naples Federico II, Via Cintia, I-80126, Naples, Italy
[2] Institute for Microelectronics and Microsystems, Unit of Naples, National Research Council, Via P. Castellino 111, I-80131, Naples, Italy
[3] Department of Chemical Sciences University of Naples Federico II, Via Cintia, I-80126, Naples, Italy

E-mail: notomist@unina.it

Received 14 December 2016, revised 28 April 2017
Accepted for publication 19 May 2017
Published 19 July 2017

Abstract

Fullerenes, allotropic forms of carbon, have very interesting pharmacological effects and engineering applications. However, a very low solubility both in organic solvents and water hinders their use. Fullerene C60, the most studied among fullerenes, can be dissolved in water only in the form of nanoparticles of variable dimensions and limited stability. Here the effect on the production of C60 nanoparticles by a native and denatured hen egg white lysozyme, a highly basic protein, has been systematically studied. In order to obtain a denatured, yet soluble, lysozyme derivative, the four disulfides of the native protein were reduced and exposed cysteines were alkylated by 3-bromopropylamine, thus introducing eight additional positive charges. The C60 solubilizing properties of the modified denatured lysozyme proved to be superior to those of the native protein, allowing the preparation of biocompatible highly homogeneous and stable C60 nanoparticles using lower amounts of protein, as demonstrated by dynamic light scattering, transmission electron microscopy and atomic force microscopy studies. This lysozyme derivative could represent an effective tool for the solubilization of other carbon allotropes.

Supplementary material for this article is available online

Keywords: lysozyme, fullerene C60, C60 nanoparticles, protein coated nanoparticles, unfolded protein

(Some figures may appear in colour only in the online journal)

Nomenclature

AFM	atomic force microscopy
AMAC	ammonium acetate
AP	amino-propyl
CAM	carboxamidomethyl
CD	circular dichroism
DLS	dynamic light scattering
drLYS	denatured and reduced lysozyme
FWS	fullerene-water system
nLYS	native lysozyme
PDI	polydispersion index
PE	pyridyl-ethyl
TEM	transmission electron microscopy
TFE	trifluoroethanol

Introduction

Fullerenes, an allotropic form of carbon, have attracted great interest due to their peculiar structural and chemical features. A molecule of fullerene C60, the most studied among fullerenes, is composed of sixty sp^2 carbon atoms arranged in twelve pentagons and twenty hexagons forming a molecular soccer ball [1]. The presence of the five membered rings and the strongly curved surface confer to C60 properties greatly distinct from those of other allotropes of carbon with sp^2 hybridization like graphene. Electron distribution is not homogeneous with the pentagons being electron deficient and the hexagon/hexagon edges being electron rich. In the crystalline solid, C60 molecules are highly ordered with each pentagon facing a hexagon/hexagon edge of an adjacent molecule [2]. Likely, this particularly favorable packing contributes to the very low solubility of C60 (discussed below).

C60 has several engineering [3] and medical applications [4, 5]. Among engineering applications, the use of C60 as electron acceptor in solar cells is particularly interesting [6]. Moreover, it has been demonstrated that host–guest complexes of C60 with charged solubilizing agents are efficient photocurrent generators [7–10].

Pharmacological effects include antibacterial [11], antioxidant [12], liver-protective and radioprotective activity [13]. Interestingly, it has been demonstrated that pristine C60, dissolved in olive oil, can prolong the lifespan of rats [14].

However, applications of pristine C60 are hindered by its very low solubility [15]. It is relatively soluble only in a few organic solvents, such as toluene, benzene and N-methylpyrrolidone (2.8, 1.7 and 0.89 mg ml^{-1}, respectively). Its solubility in methanol, ethanol, tetrahydrofuran, acetonitrile and acetone is very low [15]. Given this low solubility it is surprising that relatively high concentrations of C60 in water can be obtained by simply stirring C60 powder in water for several weeks or a few months [11]. Interestingly, the result of such procedure is not a homogeneous solution, but rather a colloidal suspension described in literature with several different names e.g. FWS (Fullerene-Water System) [16], nC60 (nano-C60) [17], etc. The peculiar properties of these colloidal solutions have been extensively investigated. In FWS the concentration of fullerene can be higher than 1 mg ml^{-1} (~2 mM). The dimensions of C60 clusters can vary from a few nanometers to several hundred nanometers (the average size and distribution is strongly influenced by the production method). FWS are colored from light yellow to dark orange, depending on C60 concentration, whereas C60 dissolved in organic solvents, like toluene, is pink. FWS are stable for several months or even years, but quickly aggregate after the addition of salts. On the contrary, organic solvents neither induce aggregation nor extract C60 from the FWS. It has been demonstrated that FWS contains hydrated fullerene molecules with a clathrate-like structure describable with the formula $C60@\{H_2O\}_n$ [16]. The charge transfer from the oxygen of water molecules to C60 is responsible both for the change in the UV–Vis spectrum of FWS and of their acidity, in fact, hydrated C60 releases protons:

$$C60@\{H_2O\}_n = C60@\{xOH^- + yH_2O\}^{x-} + xH^+ \text{ (where } n = x + y).$$

These simple species undergo aggregation, thus generating negatively charged clusters of different diameters that can be precipitated by the addition of salts. The presence of clathrate-like structures also explains why organic solvents cannot extract C60 from FWS.

Stirring C60 powder for weeks is a simple but time consuming procedure, therefore, several authors have developed faster procedures to prepare FWS. For example, FWS can be prepared by sonication of biphasic systems water/C60-saturated toluene or by slowly diluting in water concentrated solutions of C60 in water-miscible solvents like tetrahydrofuran [11]. These procedures suffer from several drawbacks: scarce reproducibility and controllability, and the necessity to accurately remove organic solvents and their oxidation products that can be toxic thus affecting the results of biological tests [18–20].

A wide variety of solubilizing agents have been evaluated to improve the dissolution of C60 in water. One of the first agents employed for this purpose was polyvinylpyrrolidone (PVP). A typical procedure involves the dissolution of C60 in toluene and of PVP in chloroform, hence the two solutions are mixed and the solvents evaporated [21]. The solid is finally sonicated in water to obtain the C60 suspension. More recently, Andreev and co-workers demonstrated that an aqueous solution of several L-amino acids (mainly uncharged amino acids) can stabilize C60 nanoparticles obtained by dialyzing C60 dissolved in N-methylpyrrolidone [17]. Both procedures, however, require the use of organic solvents. Cyclodextrins (CDxs), mainly β ad γ, allow to solubilize C60 without using organic solvents ([22] and references therein). However, the stability of the resulting complexes is limited as they require the presence of an excess of CDxs and its removal causes the formation of large aggregates of C60. In order to overcome the instability of the complexes, Kojima and co-workers prepared poly(amidoamine) dendrimers bearing on the surface CDxs and poly(ethylene glycol) [23]. By stirring the functionalized dendrimers with C60 powder in water for two days they obtained a solution containing 2.8 μM aqueous C60 (with a C60:dendrimer ratio = 1.4:1, mol:mol). Calixarenes, similarly to CDxs, form stoichimetric complexes with C60 and can be used as solubilizing agents [7, 8]. Also several complex synthetic polymers allow the solubilization of C60 in water. For example, Sawada and co-workers synthesized fluoroalkyl end-capped acryloylmorpholine oligomers which allowed the preparation of a solution containing about 29 μM aqueous C60 in water by stirring C60 powder and the polymer for one day [24]. Up until now, scarce attention has been devoted to the use of proteins, like lysozymes and albumines, or of homo- and co-polypeptides, like poly-lysine and random co-polymers of lysine and aromatic amino acids, even if this kind of macromolecules has been successfully used to solubilize carbon nanotubes [25, 26] and graphene [27–29]. To the best of our knowledge the interaction of C60/protein has been previously studied only to determine possible biological effects of C60

rather than as a tool to improve its solubility [30]. For example, Calvaresi and coworkers determined the structure of a stoichiometric complex between C60 and a native hen egg lysozyme [31].

Native hen egg lysozyme (nLYS) is a 125-residues highly basic globular protein stabilized by four disulfides. Its structure is characterized by amphipathic α-helices at the chain termini and β-strands in the middle of the protein (see figure S1, in the supplementary data available online at stacks.iop.org/NANO/28/335601/mmedia). Reduction of disulfides of nLYS provides a reversibly unfolded protein with a low amount of tertiary and secondary structure and residues from the hydrophobic core exposed to the solvent [32–34]. However, denatured LYS has very limited solubility, especially at intermediate pH values, and is prone to form aggregates involving folding intermediates [35]. Alkylation of free cysteine residues provides an irreversibly denatured protein [36] and can also increase the solubility of the denatured form [37]. Denatured and alkylated lysozyme, from several respects, shows intermediate features between those of a native protein and of random co-polypeptides: like random co-polypeptides it is essentially unfolded with the hydrophobic residues exposed to the solvent, but unlike random copolymers it has a defined sequence and in some conditions it is prone to recover a relevant amount of native-like secondary structure [36], in particular the α-helices at the N- and C-termini [38].

Here we show that hen egg lysozyme, both in the native and denatured state, is a very efficient C60 solubilizing agent allowing the preparation of a high concentration of FWS in the absence of any organic solvent, detergent or synthetic polymer. In particular, we show that through a simple procedure it is possible to obtain a denatured, but highly soluble, lysozyme derivative whose C60 solubilizing/stabilizing properties are superior to those of the native protein allowing preparation of more homogeneous C60 nanoparticles using lower amounts of protein. This lysozyme derivative could represent an effective tool for the solubilization of other carbon allotropes.

Experimental section

Preparation of denatured and reduced hen egg white lysozyme

Gallus gallus lysozyme (powder, Sigma Aldrich) was dissolved at the final concentration of 14 mg ml^{-1} in 0.1 M Tris-Acetate pH 8.4, 10 mM EDTA, 6 M Guanidine-HCl (Gu-HCl) and 25 mM DTT. The solution was purged with N_2 and incubated at 37 °C for 3 h. The reaction was blocked by acidifying to pH 4.5 with glacial acetic acid. The protein solution was dialyzed against 0.1 M acetic acid at 4 °C and centrifuged at 16 000 g for 30 min at 4 °C. Finally, the soluble lysozyme was lyophilized and stored at −80 °C until needed.

Cysteine residues modification

The alkylating agents used were: 3-bromopropylamine hydrobromide, iodoacetamide and 4-vinylpyridine, all from Sigma-Aldrich. The optimal molar ratio between cysteine and BPA was found to be 1:110 in 0.2 M Tris-HCl pH 9.5, 7 mM EDTA, 6 M Gu-HCl. The optimal conditions for reaction with iodoacetamide were 0.2 M MES pH 6.2, 7 mM EDTA, 6 M Gu-HCl with a ratio cysteines:iodoacetamide = 1:10. The reaction was incubated over night at room temperature. 4-vinylpiridine was added to denatured lysozyme in 0.1 M Tris HCl pH 8.5, 7 mM EDTA, 6 M Gu-HCl, with a ratio cysteine: 4-vinylpiridine = 1:40 and incubated over night at room temperature. All the solutions were purged with N_2 before the incubation. After incubations, the reactions were blocked by adding β-mercaptoethanol in a molar ratio of 2:1 with respect to the alkylating agents and by acidifying the solutions to pH 4.5 with glacial acetic acid. Solutions were then dialyzed against 50 mM acetic acid at 4 °C. Any insoluble material was removed by centrifugation at 16 000 g at 4 °C for 30 min and supernatants, containing alkylated lysozyme solutions, were recovered by lyophilization and stored at −80 °C until needed.

Solubility of alkylated lysozymes as function of pH

The different forms of alkylated lysozyme (AP-LYS, PE-LYS and CAM-LYS) were dissolved in 0.1 M Acetic Acid pH 3.0, 0.1 M Tris-acetate pH 5.0 and 0.1 M Tris-acetate pH 7.0 at final concentration of 1.5 mg ml^{-1}. The samples were incubated overnight at room temperature and centrifuged at 16 000 g for 1 h at 4 °C. The concentration of supernatants was determined by UV–Vis spectroscopy. Absorption spectra were acquired on a UV–Vis spectrophotometer Cary 100 Scan using a quartz cell (1 cm optics).

MALDI mass spectrometry

Matrix assisted laser desorption ionization time of flight (MALDI-TOF) spectra were acquired by using a 4800 MALDI-TOFTOF (Applied Biosystems, Framingham, MA, USA). Aliquots of samples (1 μl) were directly mixed on the plate sample holder with an equal volume of the Sinapinic acid matrix dissolved in 70% ACN, 30% formic acid 0.1% at a concentrations of 50 mg ml^{-1} to obtain a better signal-to-noise ratio. The analyses were performed in the positive ion mode, setting the instruments in the reflector mode, in the mass range 5000–20 000 m/z. A laser pulse voltage power of 3500 V was applied to improve the detection of larger compounds in the MS spectra. Each spectrum was obtained by summing 5000 laser shots at 337 nm. Raw data were analyzed using the Data Explorer Software (Applied Biosystems, Framingham, MA, USA), version 4.9, build 115 and reported as average masses.

Polyacrylamide Gel Electrophoresis (PAGE)

AP-LYS was analyzed on a 12% polyacrylamide gel containing 50 mM sodium acetate pH 4.5 and 2 M urea. The

loading buffer contained 50 mM sodium acetate pH 4.5, 2 M urea and 10% glycerol. The running buffer contained 50 mM sodium acetate pH 4.5 and 2 M urea. The run was conducted for 3 h at 150 V and room temperature.

CD spectroscopic analyses

Circular dichroism (CD) measurements were performed on a Jasco J815 spectropolarimeter (Jasco, Essex, UK), equipped with a temperature control system, using a 1 mm quartz cell in the far-UV range 194–260 nm (50 nm min^{-1} scan speed). Each spectrum was the average of three scans with the background of the buffer solution subtracted. Measurements were performed at 25 °C at a protein concentration of 0.3 mg ml^{-1} in 10 mM sodium phosphate buffer pH 7.4. Raw spectra were corrected for buffer contribution and converted to mean residue ellipticity, θ (mdeg cm^2 $dmol^{-1}$). Estimation of the secondary structure was carried out according to the variable selection method (CDSSTR) using DICHROWEB [39].

Preparation of C60 solution with AP-LYS and native LYS

C60 aqueous solutions were prepared in batches of 5 ml of 10 mM ammonium acetate (AMAC) pH 5.0 by mixing C60 powder (Sigma-Aldrich) and 0.05–0.5 mg ml^{-1} of AP-LYS/nLYS, using a medium power tip sonicator (Sonoplus, Bandelin, Germany) in an ice bath. The suspension was centrifuged at 16 000 g for 10 min at 4 °C to remove undissolved C60 powder. The UV–Vis spectra of the supernatant were measured using UV–Vis spectrophotometer Cary 100 Scan. The concentration of aqueous C60 was determined using the absorption coefficient value at 343 nm (68 000 M^{-1} cm^{-1}) [16].

DLS and Zeta potential measurements

The size of C60 nano-aggregates was quantified by dynamic light scattering (DLS), using a Malvern Zetasizer system (Zetasizer Nano ZS), which measures size distribution and Zeta potential value.

Transmission electron microscopy (TEM) characterization

Transmission electron microscopy measurements were recorded on a JEOL JEM 1011 microscope operating at an accelerating voltage of 100 KV. A droplet of the C60 solution was directly deposited on a microscope grid and analyzed.

Atomic force microscopy (AFM) characterization

A XE-100 AFM (Park Systems) was used for imaging of nanoparticles. Surface imaging was obtained in non-contact mode using silicon/aluminum coated cantilevers (PPP-NCHR 10M; Park Systems; tip radius less than 10 nm) 125 μm long with a resonance frequency of 200 to 400 kHz and nominal force constant of 42 N m^{-1}. The scan frequency was typically 0.5 Hz per line. When necessary, the AFM images were processed by flattening, in order to remove the background slope, and the contrast and brightness were adjusted.

Muscovite mica of about 1 cm^2 surface was used as substrate in AFM measurements. Muscovite mica surfaces are typically used as AFM substrate due to their perfect cleavage along ⟨001⟩ crystalline plane, yielding large atomically flat areas. Mica was freshly cleaved using adhesive tape prior to each deposition in order to get perfect cleanliness. Mica flatness is less than 0.5 nm of root-mean-square (r.m.s.) roughness for a 1000 × 1000 nm^2 surface area.

Two microliters aliquots of sample/imaging buffer were directly deposited by casting onto freshly cleaved muscovite mica. After 2 min, every sample was gently washed with deionized water and then dried by evaporation at room temperature under a ventilated fume hood.

Solubility of LYS/C60 nanoparticles

The LYS/C60 dispersions were dissolved in different buffers, 10 mM AMAC pH 5.0, 10 mM MOPS pH 7.4 and 10 mM NaP pH 7.4, in the presence and the absence of 150 mM NaCl, at the final concentration of 10 μM. After the overnight incubation at room temperature, the dispersions were centrifuged at 4000 g for 10 min at 4 °C and the supernatants were analyzed by UV–Vis measurements to quantify the concentration of C60 in solution as described above.

Cell culture and cytotoxicity assay

HaCaT and HeLa cells (ATCC) were cultured in Dulbecco's Modified Eagle's Medium (Sigma-Aldrich, St Louis, Mo, USA), supplemented with 10% fetal bovine serum (HyClone), 2 mM L-glutamine and antibiotics, all from Sigma-Aldrich, in a 5% CO_2 humidified atmosphere at 37 °C. To evaluate cell viability, the Alamar Blue assay was used. This assay is based on the reduction potential of metabolically active cells on the dye which will produce a fluorescent product. Cells (HaCaT,16 000/cm^2, and HeLa,6000/cm^2) were seeded in transparent well plates and exposed to LYS/C60 nanoparticles (ratio 1:10) at concentrations ranging from 0.5 to 3 μM for 24 and 48 h. At the end of each incubation, AlamarBlue® reagent (Invitrogen) was added in each well and incubated for 3 h at 37 °C. The fluorescence intensity was measured at an emission wavelength of 585 nm and an excitation wavelength of 570 nm using a plate reader (Synergy HTX Multi-Mode Reader-BIOTEK). Cell survival was expressed as the percentage of viable cells in the presence of the nanoparticles compared to controls. Two groups of cells were used as control, i.e. untreated cells and cells supplemented with identical volumes of buffer. Each sample was tested in three independent analyses, each carried out in triplicate. Quantitative parameters were expressed as the mean value ± SD. Significance was determined by student's t-test at a significance level of 0.05.

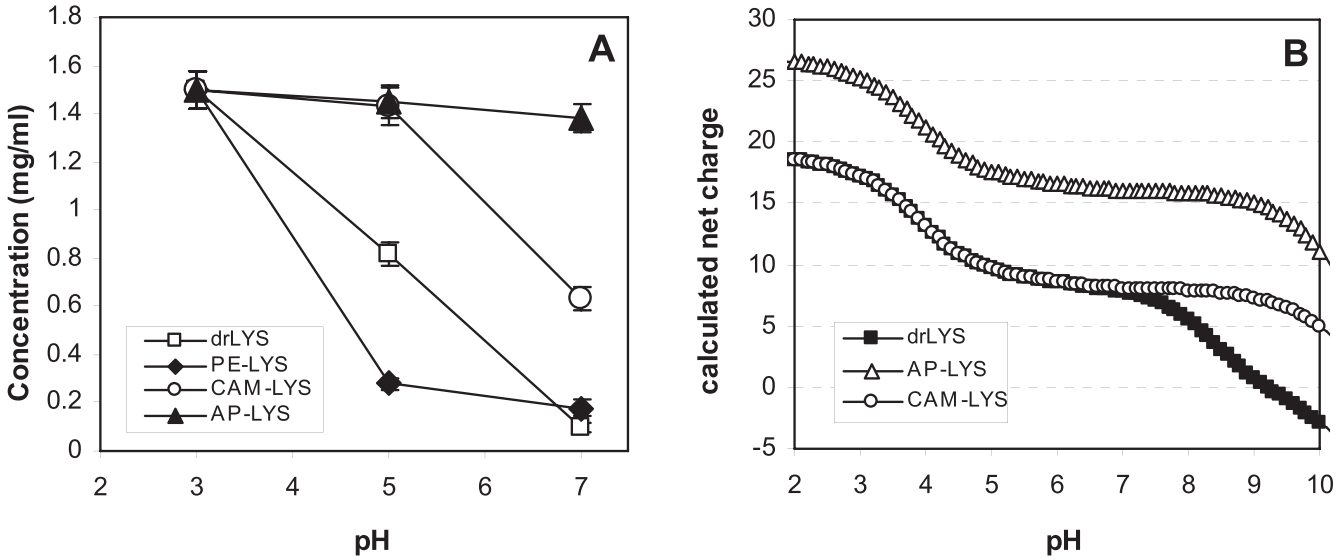

Figure 1. Solubility and predicted net charge of drLYS and its derivatives as function of pH. Filled squares, drLYS; empty diamonds, PE-LYS; empty circles, CAM-LYS; empty triangles, AP-LYS.

Results and discussion

Preparation and characterization of denatured alkylated-lysozymes

We first prepared alkylated derivatives of denatured lysozyme and compared their solubility to that of denatured and reduced lysozyme (drLYS). Three well known cysteine modifying reagents were chosen—iodoacetamide, vinylpyridine [40] and 3-bromopropylamine [41]—which allow to add to the cysteine side-chain three groups with different charge and hydrophylicity (figure S2, in supplementary data): carboxamidomethyl group is hydrophilic and uncharged in a wide range of pH values; pyridyl-ethyl group is positively charged at acidic pH but uncharged and with low polarity at neutral or alkaline pH (as comparison the pKa of 4-methylpyridine is 6.1 [42]); amino-propyl group is very hydrophilic and positively charged in a wide range of pH values.

nLYS was denatured, reduced and lyophilized to obtain drLYS as described in the Materials and Methods section, hence the exposed cysteines were alkylated with the appropriate reagents to obtain the carboxamidomethyl-derivative (CAM-LYS), the pyridyl-ethyl-derivative (PE-LYS), and the amino-propyl-derivative (AP-LYS). The content of free cysteines was determined by the Ellman test and found to always be lower than 7%. In order to determine the solubility as a function of pH, drLYS and the three derivatives were incubated at 1.5 mg ml^{-1} in acetic acid 0.1 M pH 3.0, Tris acetate 0.1 M pH 5.0 and Tris acetate 0.1 M pH 7.0. After removal of aggregate material by centrifugation, the concentration of the proteins in the supernatants was measured spectrophotometrically. As shown in figure 1(A), at pH 3.0 all the proteins showed a solubility higher than 1 mg ml^{-1}, whereas, increasing the pH resulted in a significant reduction of the solubility of drLYS and PE-LYS. Only AP-LYS showed a solubility higher that 1 mg ml^{-1} at all the pH values analyzed. These results are likely related to the amount of the net positive charge and to the hydrophylicity of the group appended to cysteine side chains. At pH 3 glutamate residues ($pK_a = \sim 4.1$) and at lesser extent aspartate residues ($pK_a = \sim 3.9$) are not ionized so that all the proteins have a high net positive charge (figure 1(B)) which likely prevents aggregation. At pH values higher than 4, the ionization of the acidic residues significantly reduce the charge thus decreasing the solubility. At all the pH values in the range 3–7 the net charge of AP-LYS is eight units higher than those of drLYS and CAM-LYS. Surprisingly, the solubility of PE-LYS is lower than that of CAM-LYS and even of that of drLYS, a result likely due to the hydrophobicity of the pyridyl-ethyl moiety.

On the basis of these results we selected AP-LYS for further characterization. The average mass of AP-LYS, determined by MALDI mass spectrometry was found to be 14 774.36 Da (figure S3, in supplementary data), in good agreement with the expected mass of a lysozyme molecule with the eight cysteine residues bound to propylamino-groups (14 771.02 Da).

In order to confirm the unfolded nature of AP-LYS, we used two complementary techniques, non-denaturing gel electrophoresis and circular dichroism (CD).

In the absence of detergents, the migration of proteins in polyacrylamide gels depends on the net charge and hydrodynamic size of the protein, therefore, for proteins of a similar charge and number of amino acids, the migration is strongly influenced by the conformation: a folded globular protein, being compact, is expected to migrate faster than the unfolded form. As expected (figure S4, in supplementary data), migration of AP-LYS toward the cathode was significantly slower that that of nLYS, in spite of the fact that AP-LYS has a higher positive charge, thus indicating that the hydrodynamic size of AP-LYS is higher than that of nLYS.

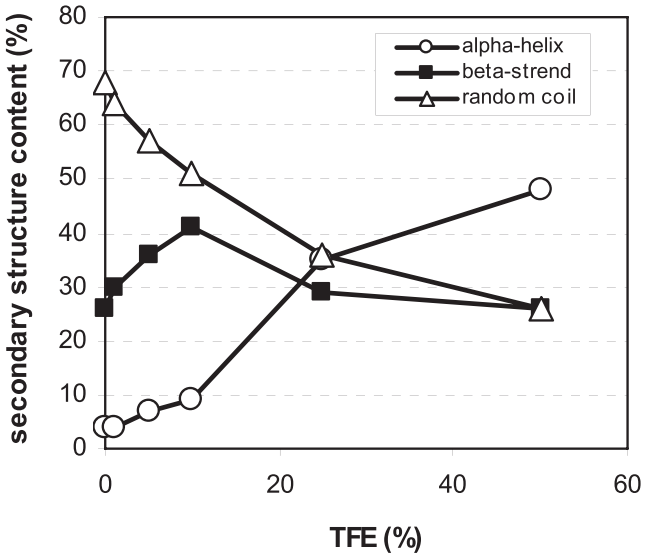

Figure 2. Secondary structure content of AP-LYS as function of the TFE concentration. Empty circles, α-helix; filled squares, β-strand; empty triangles, random coil.

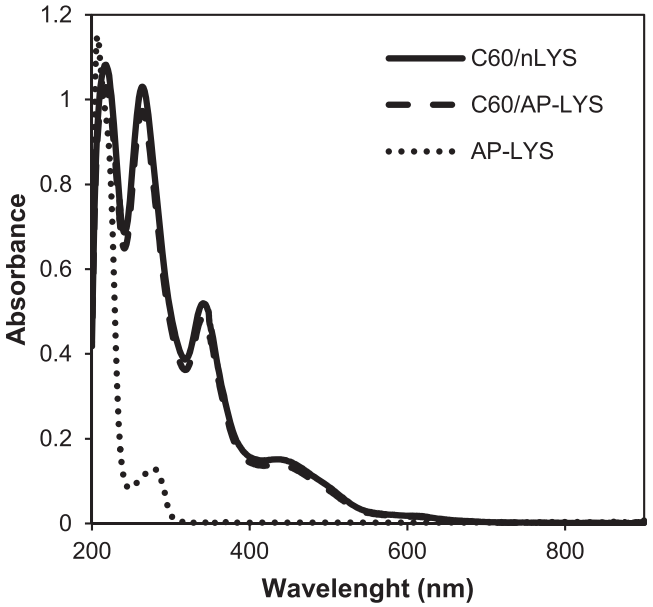

Figure 3. UV–Vis spectra of AP-LYS (dotted line) and aqueous C60 obtained by sonication of C60 powder in the presence of AP-LYS (dashed line) or nLYS (solid line). Concentrations of AP-LYS, C60 obtained in the presence of AP-LYS and C60 obtained in the presence of nLYS were 0.05 mg ml^{-1}, 7.12 μM and 7.62 μM, respectively.

The dichroic spectrum of AP-LYS was recorded at increasing concentrations (0 to 50% v/v) of trifluoroethanol (TFE) as TFE is frequently used as co-solvent in CD analysis to unmask the secondary structure propensity of peptides [43, 44] and/or to mimic the effect of hydrophobic environments like cell membranes [45–48]. In the absence of TFE, AP-LYS was essentially unfolded with only a limited amount of β-structure (figure 2). Increasing the concentration of TFE caused an increase of the α-helical content up to almost 50%, a value close to that of nLYS (figure 2).

This behavior is very similar to that of other previously investigated denatured lysozyme derivatives, namely S-carboxymethylated and S-methylated lysozymes [36]. It is worth noting that Yang and co-workers, analyzing the secondary structure of four long peptides covering the entire sequence of LYS, demonstrated that the N-terminal (residues 1–40) and C-terminal (residues 84–129) regions of lysozyme, which are helical in the native protein, are also responsible for the helical content observed in denatured LYS [38]. Therefore, it is also likely that the helical content observed in AP-LYS is due to the folding of the chain termini in the presence of TFE.

Solubilization of C60

In order to verify the effect of nLYS and AP-LYS on the production of FWS, the proteins dissolved in 10 mM ammonium acetate were mixed with C60 powder at protein/C60 ratios of 1:10, 1:1 and 10:1 (w:w) and the suspensions were sonicated for increasing times (up to three hours). At appropriate time intervals, aliquots were centrifuged at 16 000 g for 10 min to remove unsolubilized material and the supernatants were analyzed by UV-Vis spectroscopy. The C60 powder sonicated in the absence of protein provided clear solutions without any detectable aqueous fullerene, whereas all the samples containing nLYS and AP-LYS showed a bright yellow color typical of FWS. The UV-Vis spectra of these samples showed three maximum at 219, 265 and 344 nm, as well as a weak broad peak between 400 and 500 nm (figure 3) in agreement with the previously reported spectra of FWS [16]. The concentration of aqueous C60 was determined by the absorbance at 343 nm [16].

The concentration of C60 increased with the sonication time for both proteins and at all the protein/C60 ratios (figure 4). It is interesting to note that in the case of nLYS the highest concentration of soluble C60 was obtained at the highest protein:C60 powder ratio (figure 4(A)), whereas, in the case of AP-LYS the highest amount of C60 in solution was obtained at the lowest ratio (figure 4(B)) and was comparable to that obtained using the highest amount of nLYS. The yields of solubilized material are reported in table 1. The supernatants were stored at 4 °C for at least one year without changes in the UV-Vis spectrum.

To characterize the FWS we performed dynamic light scattering (DLS) and Zeta potential measurements.

DLS measurements, as expected, showed the presence of nanoparticles with diameters in the range 50–500 nm (figures 5(A) and (B)). Again, nLYS and AP-LYS showed opposite behaviors, as, in the case of the denatured protein the smallest nanoparticles were obtained at the lowest AP-LYS/C60 ratio, whereas nLYS provided small nanoparticles only at the highest ratios. Except at the highest AP-LYS/C60 ratio and the lowest nLYS/C60 ratio, the dimension of the nanoparticles was independent from the sonication time.

Furthermore, the polydispersion index (PDI), a measure of the heterogeneity of the particles, showed that AP-LYS

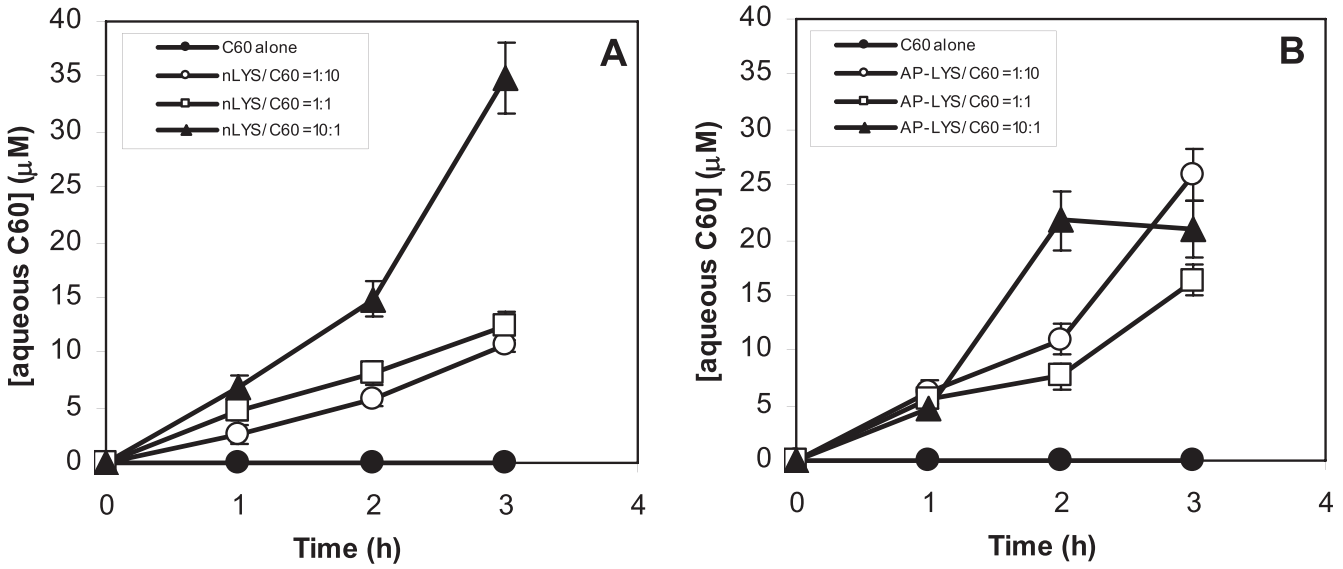

Figure 4. Concentration of aqueous C60 as function of the sonication time in the presence of nLYS (A) or AP-LYS (B). Filled circles, C60 alone; empty circles, protein/C60 = 1:10; empty squares, protein/C60 = 1:1; filled triangles, protein/C60 = 10:1.

Table 1. Yields of solubilized C60 after sonication and centrifugation at 16 000 g.

		Yields (%)		
Protein	Protein:C60	1 h	2 h	3 h
AP-LYS	1:10	0.9 ± 0.2	1.2 ± 0.2	3.8 ± 0.3
	1:1	1.1 ± 0.1	1.1 ± 0.2	2.4 ± 0.2
	10:1	0.7 ± 0.1	3.2 ± 0.4	3 ± 0.4
nLYS	1:10	0.4 ± 0.1	0.8 ± 0.1	1.6 ± 0.1
	1:1	0.7 ± 0.1	1.2 ± 0.2	1.8 ± 0.2
	10:1	1.0 ± 0.1	2.2 ± 0.2	5 ± 0.5

provided homogeneously small nanoparticles at the smallest protein: C60 powder ratio (figure 5(D)) whereas nLYS provided homogeneous nanoparticles only at high concentrations (figure 5(C)).

All the samples showed Zeta potential values in the range +10 to +35 mV, thus indicating moderate to good stability (figures 5(E) and (F)). Zeta potential values were slightly higher in the case of AP-LYS (figures 5(E) and (F)). It is worth noting that aqueous C60 nanoparticles usually have a negative Zeta potential (about −44 mV) [49], thus our results clearly indicate that C60 nanoparticles produced in the presence of AP-LYS and nLYS are protein-coated.

The observed differences between nLYS and AP-LYS are likely due to the fact that the denaturation process increases the molecular surface of AP-LYS and exposes the hydrophobic residues which are buried in the hydrophobic core of nLYS. This in turn would give AP-LYS the ability to cover a larger surface area and, possibly, a stronger interaction with the surface of the nanoparticles. Moreover, the increased net charge of AP-LYS due to the modification of the eight cysteine residues could contribute to increase the Zeta potential and the stability of the particles.

Characterization of nanoparticles by TEM and AFM

TEM and AFM analyses were performed to deeply inspect the morphology of the nanoparticles produced by solubilization of C60 in presence of nLYS and AP-LYS. Both forms of lysozyme were able to produce highly dispersed nanoparticles that could be imaged by TEM and AFM, but with some substantial differences. By looking at images reported in figures 6 and 7, it was well evident that AP-LYS strongly disaggregated C60 clusters in solution, in both volume proportions (1:10) and (10:1). Hybrid C60/AP-LYS nanoparticles appeared highly dispersed on the TEM grid and on AFM mica support, and quantitative measurements quantified size in the range of few hundreds of nanometers (100–200 nm) in width (see figures 6(A), (B)), and few tenths of nanometers in (10–20 nm) in height, as it is shown in figure 7(A). In the sample with a ratio AP-LYS/C60 = 10:1, some small agglomerates of C60/AP-LYS nanoparticles could be detected (see for example the small cluster in topographic AFM image of figure 7(B)), which were not present in the sample with a ratio AP-LYS/C60 = 1:10 (figures 6(A), (B) and 7(A)).

nLYS could also dissolve the insoluble C60 aggregates, but less effectively: the result was the formation of well-known carbon superstructures named in literature as nanohorns [50] clearly imaged by TEM (figures 6(G) and (H)) and AFM (figures 7(C) and (D)). In the sample with a ratio nLYS/C60 = 10:1 the nanohorn motif, which gave rise to large hybrid clusters (more then 1 micron width), as shown in figure 6(G), could be also evidenced at high spatial resolution by the AFM technique (figure 7(D)): from this visualization it is clear that the single nanohorn (approximately 500 nm in width and less then 1 nm height) was an ensemble of several C60-protein clusters that had not been completely solubilized by nLYS. Even the sample with a ratio nLYS/C60 = 1:10 was found to contain large agglomerates of nanoparticles, as reported in figure 6(E), and the AFM analysis of this sample

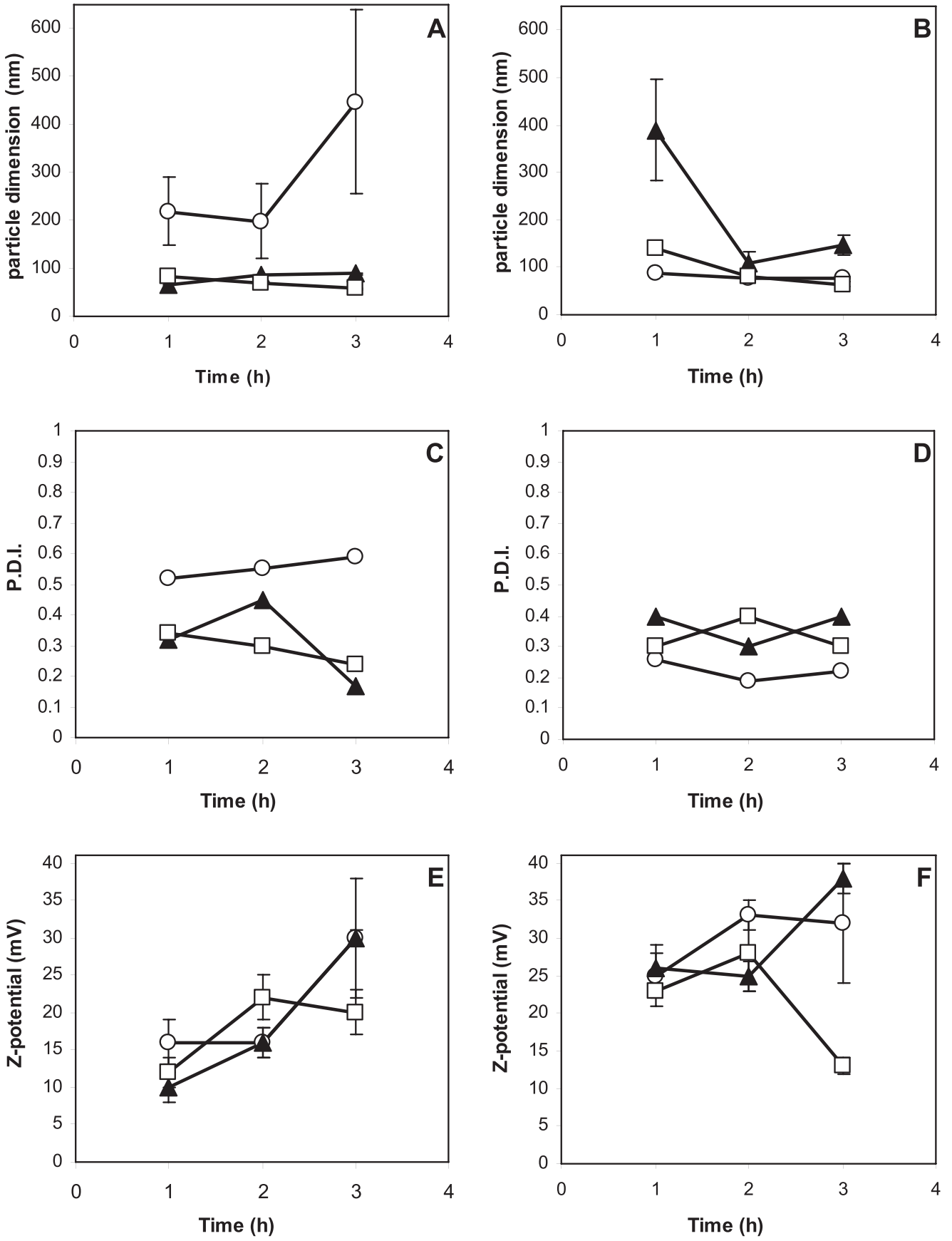

Figure 5. DLS and Zeta potential analysis of C60 nanoparticles prepared using nLYS (A), (C), (E) or AP-LYS (B), (D), (F). Empty circles, protein/C60 = 1:10; empty squares, protein/C60 = 1:1; filled triangles, protein/C60 = 10:1. Error bars are shown only when larger than the symbol.

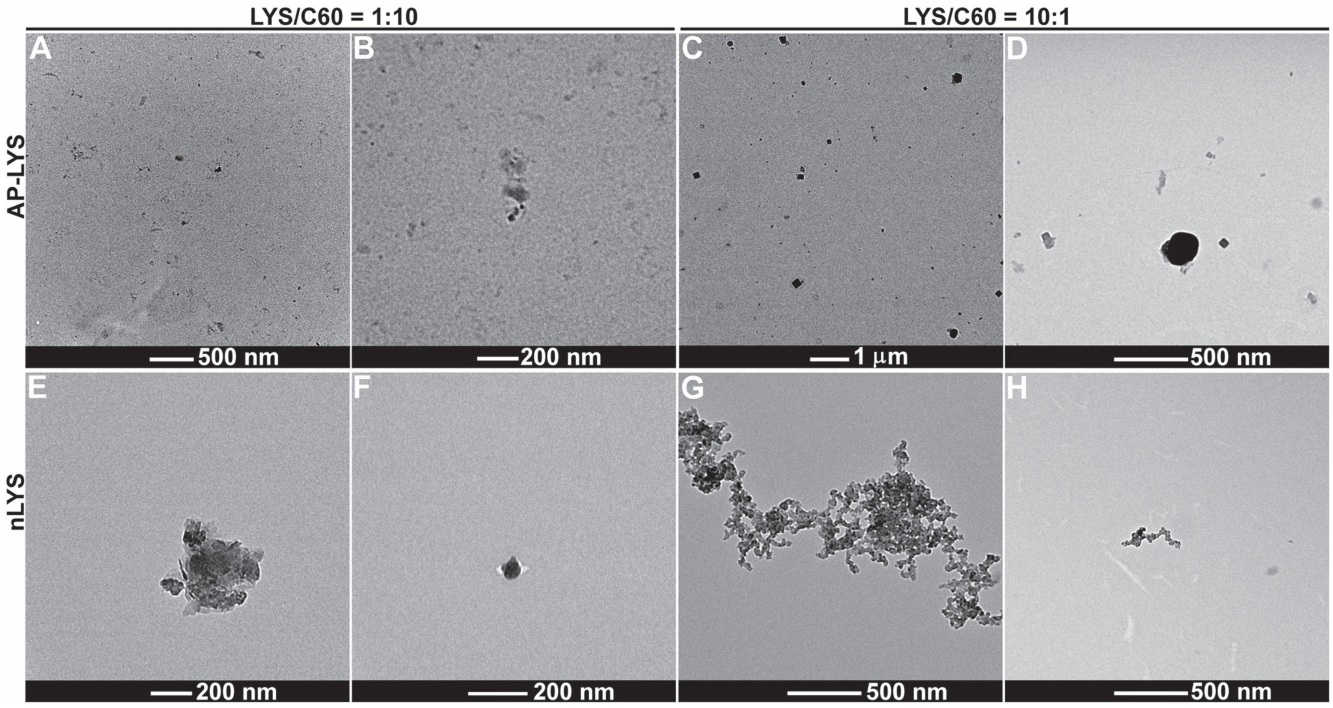

Figure 6. TEM images of nanoparticles deposited on cellulose grid from a solution of C60 and AP-LYS (A)–(D) or nLYS (E)–(F). (A), (B) AP-LYS/C60 = 1:10. (C), (D) AP-LYS/C60 = 10:1. (E), (F) nLYS/C60 = 1:10. (G), (H) nLYS/C60 = 10:1.

revealed that complex aggregates of C60-nLYS were constituted by single compacted nanohorns, easily recognizable in figure 7(C).

Solubility of the LYS/C60 nanoparticles

As it is well known that aqueous C60 quickly aggregates after the addition of salts, we analyzed the behavior of the LYS/C60 nanoparticles in the presence and absence of a physiological concentration of NaCl (150 mM) in different buffers (10 mM AMAC pH 5.0, 10 mM MOPS pH 7.4 and 10 mM NaP pH 7.4). C60 nanoparticles were diluted at a concentration of 10 μM, after 16 h at room temperature, the samples were centrifuged at 4000 g for 10 min and the concentration of C60 remaining in solution was determined spectrophotometrically.

Buffer and pH value had scarce influence on the final C60 concentration, whereas NaCl caused a significant reduction in the samples containing AP-LYS at the ratio protein/C60 of 1:10 and at a higher extent nLYS at the protein/C60 of 1:10 and 10:1 (figure 8).

Only AP-LYS at the ratio protein/C60 of 10:1 preserved the solubility of nanoparticles in the presence of NaCl (figure 8(B)). In order to determine the effects of NaCl on nanoparticles dimensions and stability, DLS and Zeta potential measurements were performed (table 2). The addition of NaCl did not significantly change the average dimensions of the particles even if, at least at pH 7.4, a significant increase of the P.D.I. –i.e. the heterogeneity– of the samples was observed. However, the most relevant effect was observed in the case of the Zeta potential values which showed a decrease to about 70% of the initial value when the pH was increased from 5 to 7.4 and a further decrease to about 50% of the initial value after the addition of NaCl. The effect of pH on Zeta potential values is a likely consequence of the reduction in the net charge of AP-LYS with increasing pH, as discussed above and shown in figure 1(B). As for the effects of NaCl, it is likely that, at high concentration of NaCl, Cl^- ions can bind to the cationic AP-LYS coating thus reducing its net charge. These findings indicate also that in the case of the nanoparticles containing an excess of AP-LYS, the presence of NaCl reduces the stability.

Biocompatibility of LYS/C60 nanoparticles

As described in the introduction, C60, and several of its derivatives, have very intriguing pharmacological activities [11–14]. However, a low toxicity is mandatory for any pharmacological application, therefore, we decided to evaluate the biocompatibility of the LYS-coated C60 nanoparticles. The biocompatibility of the samples containing LYS/C60 at a ratio of 1:10 was measured by a cell proliferation assay using the Alamar Blue dye, as described in material and methods section (figure 9). Human normal keratinocytes (HaCaT cells) and human cancer epithelial cells (HeLa cells) were exposed to increasing concentrations of either AP-LYS/C60 or nLYS/C60 nanoparticles (0.5–3 μM) for 24 (figures 9(A), (C)) and 48 h (figures 9(B), (D)). No alteration of cell viability was observed in cells incubated with both nanoparticles,

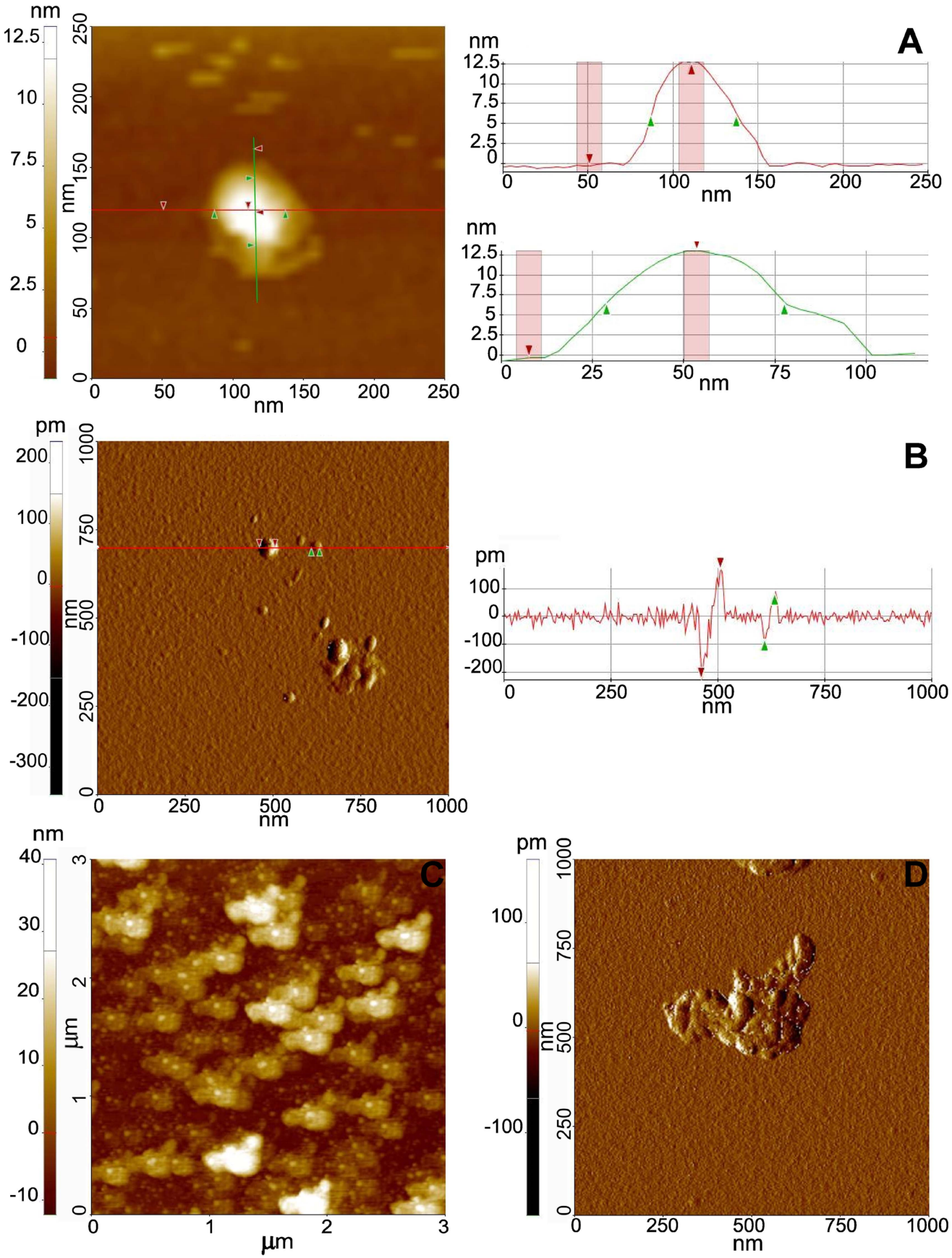

Figure 7. AFM topographic images of samples deposited on mica from a solution of C60 and AP-LYS (A), (B) or nLYS (C), (D). (A) AP-LYS/C60 = 1:10. (B) AP-LYS/C60 = 10:1. (C) nLYS/C60 = 1:10. (D) nLYS/C60 = 10:1. Panels A and B show on the right cross sections taken at the red or green lines indicated in AFM images.

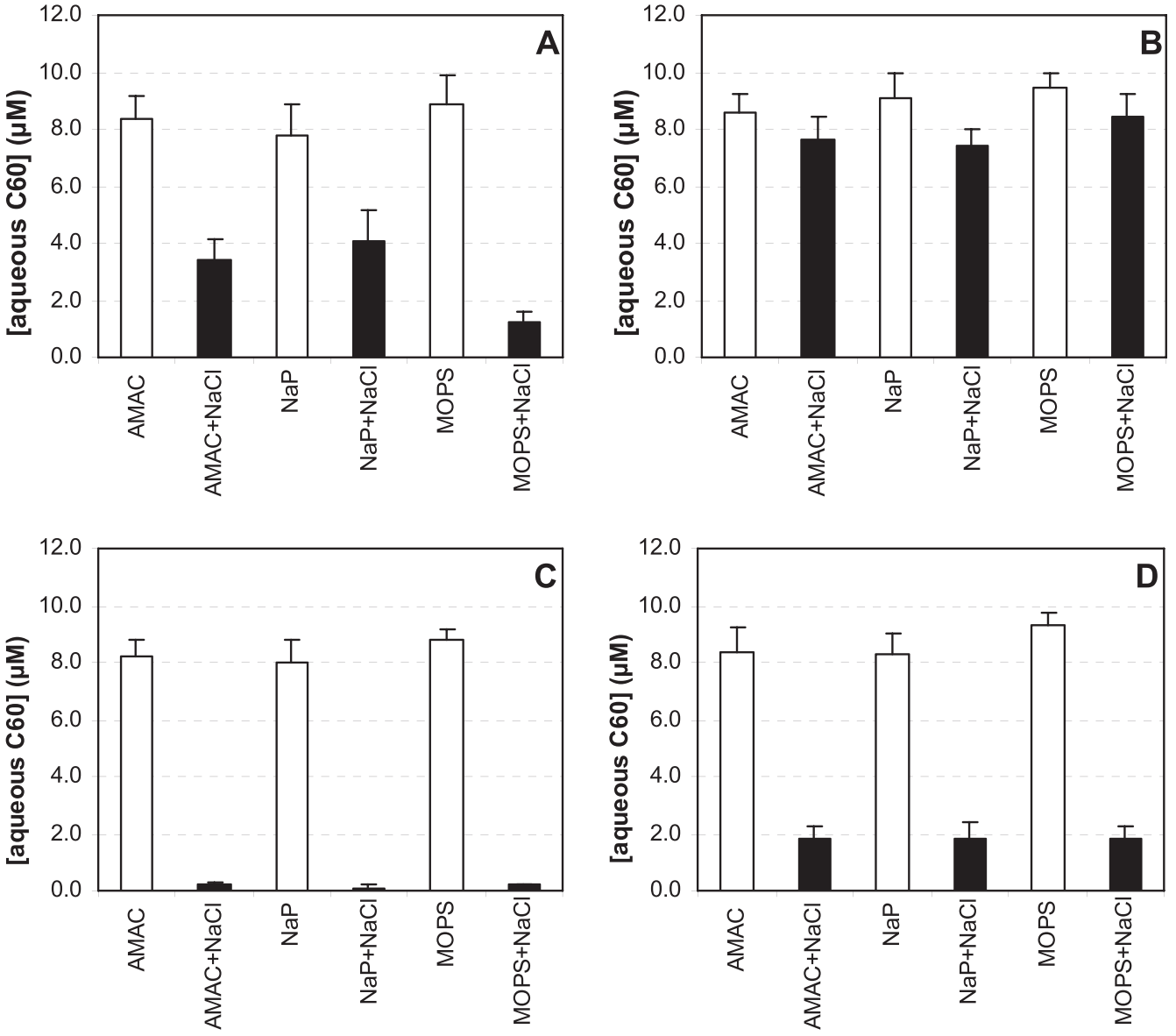

Figure 8. Response to buffer and ionic strength of the C60 nanoparticles prepared using AP-LYS (A), (B) or nLYS (C), (D). (A) AP-LYS/C60 = 1:10. (B) AP-LYS/C60 = 10:1. (C) nLYS/C60 = 1:10. (D) nLYS/C60 = 10:1. White bars, concentration of C60 after incubation in buffers without NaCl; black bars, concentration of C60 after incubation in buffers containing NaCl (150 mM). AMAC, 10 mM AMAC pH 5.0; MOPS, 10 mM MOPS pH 7.4; NaP, 10 mM sodium phosphate pH 7.4.

with respect to untreated cells at any of the concentrations tested, up to 48 h incubation ($p > 0.05$).

Conclusions

Denaturation of globular proteins has a profound impact not only on their biological properties but also on their chemico-physical properties, in fact, unfolding exposes the hydrophobic residues of the protein core to the solvent and drastically increases the accessible surface and the flexibility of the protein. On the other hand, denatured proteins retain a significant amount of secondary structures and/or sequences prone to regain secondary structures. The increase in surface hydrophobicity and the presence of amphipathic secondary structure elements make unfolded proteins very prone to aggregation thus impairing their use in material sciences. Here we have shown that, by a careful choice of the alkylating agent, hen egg white lysozyme can be converted to an irreversibly denatured yet very soluble protein. CD data demonstrated that AP-LYS is essentially unfolded in water but prone to regain a significant content of helical structure, whereas urea PAGE confirmed that its hydrodynamic volume is higher than that of the native protein. Even if both the native lysozyme and AP-LYS are proven to effectively promote the sonication mediated solubilization of C60 in water, AP-LYS is a more convenient solubilizer for several reasons. DLS, TEM and AFM analysis showed that AP-LYS mediates

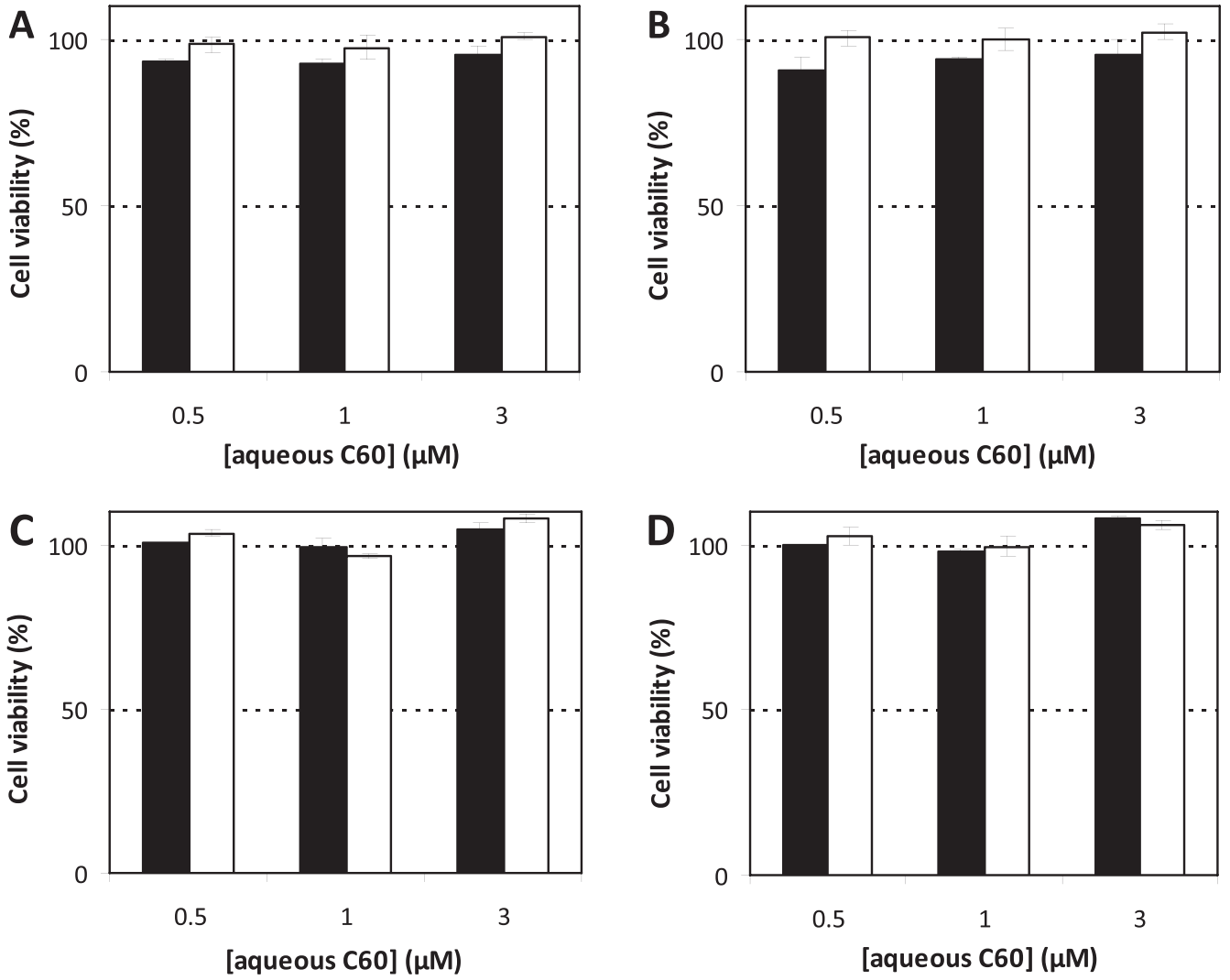

Figure 9. Time-course of the effects of LYS/C60 nanoparticles on human cells after 24 h (A), (C) and 48 h (B), (D) by the Alamar Blue assay. HeLa cells (black bars) and HaCaT cells (white bars) were incubated with increasing concentrations (0.5–3 μM) of either AP-LYS/C60 (A), (B) or nLYS/C60 (C), (D) nanoparticles. Error bars correspond to the SD values of three independent experiments carried out with triplicate determinations.

the formation of smaller and more homogeneous (monodisperse) nanoparticles than the native proteins. Even more interestingly, AP-LYS works effectively at low concentrations, indeed the best performance was obtained at a ratio AP-LYS/C60 = 1:10. Moreover, the Zeta potential values of the particles coated by AP-LYS were slightly higher than those of the particles coated by native protein, thus suggesting a higher stability in water. This was further confirmed by the higher resistance to the salt induced precipitation of the AP-LYS coated particles.

The observed differences between the native and the denatured protein are likely to be due to the increase in the molecular surface and flexibility caused by the denaturation process. The increased surface would enable AP-LYS to cover a larger area at the surface of the nanoparticle whereas the increased flexibility could allow AP-LYS to interact more effectively with the surface of the nanoparticles. The increased net charge in AP-LYS could contribute to increase the Zeta potential and the stability of the particles. It is less

Table 2. DLS and Zeta potential measurements of LYS/C60 nanoparticles (protein/C60 = 10:1) in different buffers with and without NaCl (150 mM).

Buffer	DLS (nm)	P.D.I.	Zeta potential (mV)
AMAC[a] (pH 5.0)	88 ± 3	0.23 ± 0.01	34 ± 2
AMAC[a] + NaCl (pH 5.0)	97 ± 5	0.21 ± 0.05	16.2 ± 0.4
NaP[b] (pH 7.4)	87 ± 1	0.21 ± 0.02	21.1 ± 0.5
NaP[b] + NaCl (pH 7.4)	95 ± 3	0.37 ± 0.06	16.1 ± 0.8
MOPS[c] (pH 7.4)	76 ± 1	0.22 ± 0.01	26 ± 4
MOPS[c] + NaCl (pH 7.4)	84 ± 2	0.38 ± 0.05	17 ± 1

[a] 10 mM AMAC pH 5.0. This is the buffer used for the preparation and storage of the nanoparticles.
[b] 10 mM NaP pH 7.4.
[c] 10 mM MOPS pH 7.4.

clear which molecular interactions mediate the binding of AP-LYS to the surface of the particles. Previous studies on native lysozyme suggested that it can interact with carbon surfaces both through hydrophobic interactions, mediated by hydrophobic patches present on the lysozyme surface, and electrostatic interactions between the basic residues on the protein and the negative charges present on several carbon surfaces. As the denaturation and chemical modification increase both the positive charge and the exposed hydrophobic surface, it could be hypothesized that both interactions could contribute to binding in the case of AP-LYS also.

Very intriguingly, the AP-LYS- coated C60 nanoparticles shown to be non-toxic for two human cell lines, thus suggesting that they could find pharmacological applications e.g. in photodynamic therapy. In general, our work demonstrates that AP-LYS is a very promising solubilizing agent which may find a future application in the preparation of soluble derivatives of other carbon materials like nanotubes and graphene.

Acknowledgments

This work was supported by grants FFC#11/2013 and FFC#12/2014 from 'Italian Cystic Fibrosis Research Foundation' (http://fibrosicisticaricerca.it). The authors are grateful to Professor Paola Giardina for the critical reading of the manuscript.

References

[1] Geckeler K E and Samal S 1999 Syntheses and properties of macromolecular fullerenes, a review *Polymer Int.* **48** 743–57
[2] David W I F, Ibberson R M, Matthewman J C, Prassides K, Dennis T J S, Hare J P, Kroto H W, Taylor R and Walton D R M 1991 Crystal structure and bonding of ordered C60 *Nature* **353** 147–9
[3] Pilehvar S and De Wael K 2015 Recent advances in electrochemical biosensors based on fullerene-C60 nanostructured platforms *Biosensors* **5** 712–35
[4] Bakry R, Vallant R M, Najam-ul-Haq M, Rainer M, Szabo Z, Huck C W and Bonn G K 2007 Medicinal applications of fullerenes *Int. J. Nanomedicine* **2** 639–49
[5] Partha R and Conyers J L 2009 Biomedical applications of functionalized fullerene-based nanomaterials *Int. J. Nanomedicine* **4** 261–75
[6] Günes S, Neugebauer H and Sariciftci N S 2007 Conjugated polymer-based organic solar cells *Chem. Rev.* **107** 1324–38
[7] Hatano T, Ikeda A, Akiyama T, Yamada S, Sano M, Kanekiyo Y and Shinkai S 2000 Facile construction of an ultra-thin [60]fullerene layer from [60]fullerene–homooxacalix[3]arene complexes on a gold surface *J. Chem. Soc., Perkin Trans.* **2** 909–12
[8] Ikeda A, Hatano T, Shinkai S, Akiyama T and Yamada S 2001 Efficient photocurrent generation in novel self-assembled multilayers comprised of [60]fullerene-cationic homooxacalix[3]arene inclusion complex and anionic porphyrin polymer *J. Am. Chem. Soc.* **123** 4855–6
[9] Hatano T, Takeuchi M, Ikeda A and Shinkai S 2003 Facile deposition of [60]fullerene on the electrode by electrochemical oxidative polymerization of thiophene *Chem. Commun.* **3** 342–3
[10] Hatano T, Bae A H, Sugiyasu K, Fujita N, Takeuchi M, Ikeda A and Shinkai S 2003 Facile deposition of [60] fullerene and carbon nanotubes on ITO electrode by electrochemical oxidative polymerization of ethylenedioxythiophene *Org. Biomol. Chem.* **1** 2343–7
[11] Lyon D Y, Adams L K, Falkner J C and Alvarezt P J 2006 Antibacterial activity of fullerene water suspensions: effects of preparation method and particle size *Environ. Sci. Technol.* **40** 4360–6
[12] Gharbi N, Pressac M, Hadchouel M, Szwarc H, Wilson S R and Moussa F 2005 [60] fullerene is a powerful antioxidant *in vivo* with no acute or subacute toxicity *Nano Lett.* **5** 2578–85
[13] Andrievsky G V, Bruskov V I, Tykhomyrov A A and Gudkov S V 2009 Peculiarities of the antioxidant and radioprotective effects of hydrated C60 fullerene nanostuctures *in vitro* and *in vivo Free Radic. Biol. Med.* **47** 786–93
[14] Baati T, Bourasset F, Gharbi N, Njim L, Abderrabba M, Kerkeni A, Szwarc H and Moussa F 2012 The prolongation of the lifespan of rats by repeated oral administration of [60] fullerene *Biomaterials* **33** 4936–46
[15] Ruoff R S, Tse D S, Malhotra R and Lorents D C 1993 Solubility of fullerene (C60) in a variety of solvents *J. Phys. Chem.* **97** 3379–83
[16] Andrievsky G V, Klochkov V K, Bordyuh A B and Dovbeshko G I 2002 Comparative analysis of two aqueous-colloidal solutions of C60 fullerene with help of FTIR reflectance and UV–Vis spectroscopy *Chem. Phys. Lett.* **364** 8–17
[17] Andreev S M, Purgina D D, Bashkatova E N, Garshev A V, Maerle A V and Khaitov M R 2014 Facile preparation of aqueous fullerene C60 nanodispersions *Nanotechnol. Russia* **9** 369–79
[18] Andrievsky G, Klochkov V and Derevyanchenko L 2005 Is the C60 fullerene molecule toxic?! *Fullerenes, Nanotubes, Carbon Nanostructures* **13** 363–76
[19] Kim K T, Jang M H, Kim J Y and Kim S D 2010 Effect of preparation methods on toxicity of fullerene water suspensions to Japanese medaka embryos *Sci. Total Environ.* **408** 5606–12
[20] Brant J, Lecoanet H, Hotze M and Wiesner M 2005 Comparison of electrokinetic properties of colloidal fullerenes (n-C60) formed using two procedures *Environ. Sci. Technol.* **39** 6343–51
[21] Yamakoshi Y N, Yagami T, Fukuhara K, Sueyoshi S and Miyata N 1994 Solubilization of fullerenes into water with polyvinylpyrrolidone applicable to biological tests *J. Chem. Soc., Chem. Commun.* **4** 517–8
[22] Ikeda A 2013 Water-soluble fullerenes using solubilizing agents, and their applications *J. Incl. Phenom. Macrocycl. Chem.* **77** 49–65
[23] Kojima C, Toi Y, Harada A and Kono K 2008 Aqueous solubilization of fullerenes using poly(amidoamine) dendrimers bearing cyclodextrin and poly(ethylene glycol) *Bioconjug. Chem.* **19** 2280–4
[24] Sawada H, Iidzuka J, Maekawa T, Takahashi R, Kawase T, Oharu K, Nakagawa H and Ohira K 2003 Solubilization of fullerene into water with fluoroalkyl end-capped amphiphilic oligomers-novel fluorescence properties *J. Colloid Interface Sci.* **263** 1–3
[25] Calvaresi M and Zerbetto F 2013 The devil and holy water: protein and carbon nanotube hybrids *Acc. Chem. Res.* **46** 2454–63
[26] Kojima M *et al* 2011 Dispersion of single-walled carbon nanotubes modified with poly-l-tyrosine in water *Nanoscale Res. Lett.* **6** 128
[27] Gravagnuolo A M, Morales-Narváez E, Longobardi S, da Silva E T, Giardina P and Merkoçi A 2015 *In situ* production of biofunctionalized few-layer defect-free microsheets of graphene *Adv. Funct. Mater.* **25** 2771–9

[28] Yang W, Ren Q, Wu Y N, Morris V K, Rey A A, Braet F, Kwan A H and Sunde M 2013 Surface functionalization of carbon nanomaterials by self-assembling hydrophobin proteins *Biopolymers* **99** 84–94
[29] Wang J, Zhao Y, Ma F X, Wang K, Wang F B and Xia X H 2013 Synthesis of a hydrophilic poly-L-lysine/graphene hybrid through multiple non-covalent interactions for biosensors *J. Mater. Chem.* B **1** 1406–13
[30] Abdulmalika A, Hibaha A, Zainya B M, Makotoc A, Daisukec I, Masakic O, Kanetoa U and Fumitosh H 2013 Preparation of soluble stable C60/human serum albumin nanoparticles via cyclodextrin complexation and their reactive oxygen production characteristics *Life Sciences* **93** 277–82
[31] Calvaresi M *et al* 2014 C60@Lysozyme: direct observation by nuclear magnetic resonance of a 1:1 fullerene protein adduct *ACS Nano* **8** 1871–7
[32] Yutani K, Yutani A, Imanishi A and Isemura T 1968 The mechanism of refording of the reduced random coil form of lysozyme *J. Biochem.* **64** 449–55
[33] Saxena V P and Wetlaufer D B 1970 Formation of three-dimensional structure in proteins. I. Rapid nonenzymic reactivation of reduced lysozyme *Biochemistry* **9** 5015–23
[34] Gekko K, Kimoto A and Kamiyama T 2003 Effects of disulfide bonds on compactness of protein molecules revealed by volume, compressibility, and expansibility changes during reduction *Biochemistry* **42** 13746–53
[35] De Bernardez Clark E, Hevehan D, Szela S and Maachupalli-Reddy J 1998 Oxidative renaturation of hen egg-white lysozyme. Folding vs aggregation *Biotechnol. Prog.* **14** 47–54
[36] Lee C L and Atassi M Z 1973 Conformation and immunochemistry of methylated and carboxymethyulated derivatives of lysozyme *Biochemistry* **12** 2690–5
[37] Yamada H, Seno M, Kobayashi A, Moriyama T, Kosaka M, Ito Y and Imoto T 1994 An S-alkylating reagent with positive charges as an efficient solubilizer of denatured disulfide-containing proteins *J. Biochem.* **116** 852–7
[38] Yang J J, Buck M, Pitkeathly M, Kotik M, Haynie D T, Dobson C M and Radford S E 1995 Conformational properties of four peptides spanning the sequence of hen lysozyme *J. Mol. Biol.* **252** 483–91
[39] Whitmore L and Wallace B A 2004 DICHROWEB, an online server for protein secondary structure analyses from circular dichroism spectroscopic data *Nucleic Acids Res.* **32** W668–73
[40] Jiang X, Shamshurin D, Spicer V and Krokhin O V 2013 The effect of various S-alkylating agents on the chromatographic behavior of cysteine-containing peptides in reversed-phase chromatography *J. Chromatogr. B Analyt. Technol. Biomed. Life Sci.* **915–916** 57–63
[41] Jue R A and Hale J E 1993 Identification of cysteine residues alkylated with 3-bromopropylamine by protein sequence analysis *Anal. Biochem.* **210** 39–44
[42] Perrin D D 1972 *Dissociation Constants of Organic Bases in Aqueous Solution, Supplement* (London: Butterworths)
[43] Kelly S M, Jess T J and Price N C 2005 How to study proteins by circular dichroism *Biochimica et Biophysica Acta (BBA) —Proteins and Proteomics* **1571** 119–39
[44] Reiersen H and Rees A R 2000 Trifluoroethanol may form a solvent matrix for assisted hydrophobic interactions between peptide side chains *Protein Eng.* **13** 739–43
[45] Carlier L, Joanne P, Khemtemourian L, Lacombe C, Nicolas P, El Amri C and Lequin O 2015 Investigating the role of GXXXG motifs in helical folding and self-association of plasticins, Gly/Leu-rich antimicrobial peptides *Biophys. Chem.* **196** 40–52
[46] Lequin O, Ladram A, Chabbert L, Bruston F, Convert O, Vanhoye D, Chassaing G, Nicolas P and Amiche M 2006 Dermaseptin S9, an alpha-helical antimicrobial peptide with a hydrophobic core and cationic termini *Biochemistry* **45** 468–80
[47] Wang L, Wang D and Li F 2014 Insight into the structures of the second and fifth transmembrane domains of Slc11a1 in membrane mimics *J. Pept. Sci.* **20** 165–72
[48] Di Natale G, Pappalardo G, Milardi D, Sciacca M F, Attanasio F, La Mendola D and Rizzarelli E 2010 Membrane interactions and conformational preferences of human and avian prion N-terminal tandem repeats: the role of copper(II) ions, pH, and membrane mimicking environments *J. Phys. Chem.* B **114** 13830–8
[49] Chen Z, Westerhoff P and Herckes P 2008 Quantification of C60 fullerene concentrations in water *Environ. Toxicol. Chem.* **27** 1852–9
[50] Karousis N, Suarez-Martinez I, Ewels C P and Tagmatarchis N 2016 Structure, properties, functionalization, and applications of carbon nanohorns *Chem. Rev.* **116** 4850–83